Supporting Information for

Covalent Organic Framework-Based Electrolytes for Fast Li^+ Conduction and High-Temperature Solid-State Lithium-Ion Batteries

Zhen Shan,[a]+ Miaomiao Wu,[a]+ Yihan Du,[a] Bingqing Xu,*[a] Boying He,[a] Xiaowei Wu,[a] Gen Zhang*[a]

[a] Key Laboratory for Soft Chemistry and Functional Materials of Ministry of Education, School of Chemical Engineering, Nanjing University of Science and Technology, Nanjing, Jiangsu 210094, China.

[+] These authors contributed equally to this work.

This paper dedication to Professor Susumu Kitagawa on the occasion of his 70th birthday

Email: *bingqingxu@njust.edu.cn (B.X.); *zhanggen@njust.edu.cn (G.Z.)

Table of contents:

1 Experimental Section

1.1 Materials and general methods

All the chemicals are commercially available, and used without further purification. All solvents were dried and distilled according to conventional methods. 2,4,6-tris(4-aminophenyl)benzene, 4,4',4''-(1,3,5-triazine-2,4,6-triyl) trianiline, and *N*, *N*-bis(4-aminophenyl)benzene-1,4-diamine were purchased from energy chemical (Shanghai, China). Bistrifluoromethanesulfonimide lithium salt (LiTFSI) and ionic liquids (1-butyl-1-methylpyrrolidinium bis(trifluoromethanesulfonyl)imide, Py14TFSI, IL) were purchased from Heowns Biochem Technologies LLC (Tianjin, China). $LiFePO_4$, super P, PVDF powders were purchased from Shenzhen Kejing Star Technology Company (Shenzhen, China).

All samples were characterized and analyzed by related techniques. PXRD patterns were collected on a Bruker D8 Advance diffractometer using Cu Kα radiation. Liquid state $^{1}H/^{13}C/^{19}F$/ nuclear magnetic resonance spectra were collected on a Bruker Advance III instrument with AS500 magnet equipped with a cryoprobe (300 MHz). All ssNMR spectra were recorded on a JEOL JNM-ECZ600R spectrometer at 14.1 T (1H: 600 MHz) and 1.0 mm rotors. SEM images were collected using a JSM-IT500HR system. Gas adsorption measurement N_2 adsorption and desorption measurements were performed at 77 K using ASAP 2020, Micromeritics Instrument Corp, USA. Pore size distributions and pore volumes were derived from the adsorption isotherms. TGA was performed using a NETZSCH STA 449F5 under flowing N_2 with 10 K min^{-1} ramp rate. Samples were heated in a Platinum pan (900 ℃, 10 ℃ min^{-1}) under a N_2 flux (60 mL min^{-1}). Fourier transform infrared (FT-IR) spectra were collected by Universal ATR accessory between the ranges of 4000 to 500 cm^{-1}.

1.2 Synthesis of monomers and COFs

Synthesis of 1,3,5-Tri(2-thienyl)benzene

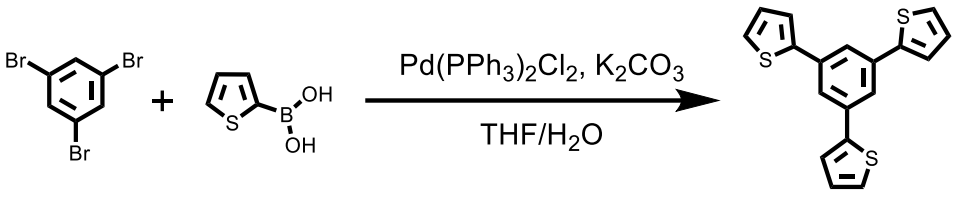

1

Under argon atmosphere, 1,3,5-tribromobenzene (3.14 g, 10 mmol), 2-thiophenylboronic acid (5.12 g, 40 mmol), and $Pd(PPh_3)_2Cl_2$ (70.2 mg, 0.1 mmol) were dissolved in anaerobic THF (30 mL), then 20 mL anaerobic aqueous K_2CO_3 solution (5 M) was added. The system was stirred at refluxing temperature for 48 h. The mixture was cooled, and extracted with DCM. The organic layer was washed with water and dried over anhydrous $MgSO_4$. After the solvent was removed, the residue was purified by silica gel column chromatography (eluent: petroleum) to give a white solid (2.5 g, yield: 77%). [1]

Synthesis of 1,3,5-Tri(4-formyl-2-thienyl)benzene (3TB)

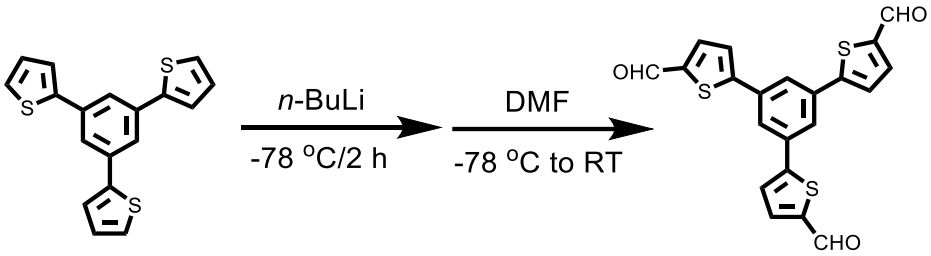

1 **3TB**

n-BuLi (2.8 mL, 2.4 M in hexane) was added dropwise to 1,3,5-Tri(2-thienyl)benzene (0.67 g, 2.1 mmol) in THF (50 mL) at -78 °C. After 2 h at -78 °C, DMF (0.8 mL, 10.5 mmol) was added at -78 °C and kept 0.5 h, and then the reaction mixture was warmed up slowly to ambient temperature overnight. The reaction was quenched with methanol. And then removed solvent under reduced pressure and the crude product was washed with MeOH to afford a pale-yellow solid,[2] compound **3TB** (0.72 g, yield: 86%), ^{1}H NMR (300 MHz, DMSO-d_6) δ (ppm): 9.97 (s, 2 H), 8.17 (s, 3 H), 8.13 (d, 3 H), 8.07 (s, 3 H), which was used for the next step without further purification. [2]

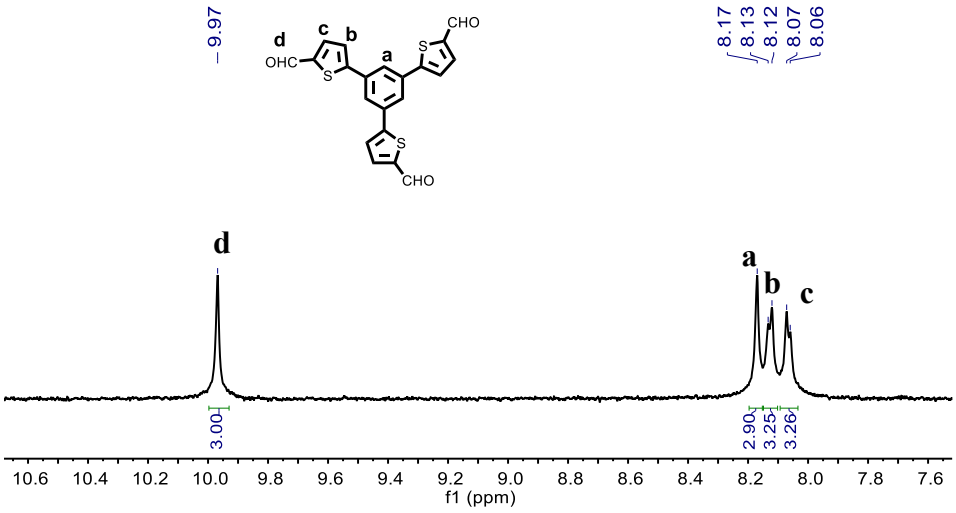

Figure S1. ^{1}H NMR spectra of **3TB**

Synthesis of COF-NUST-7

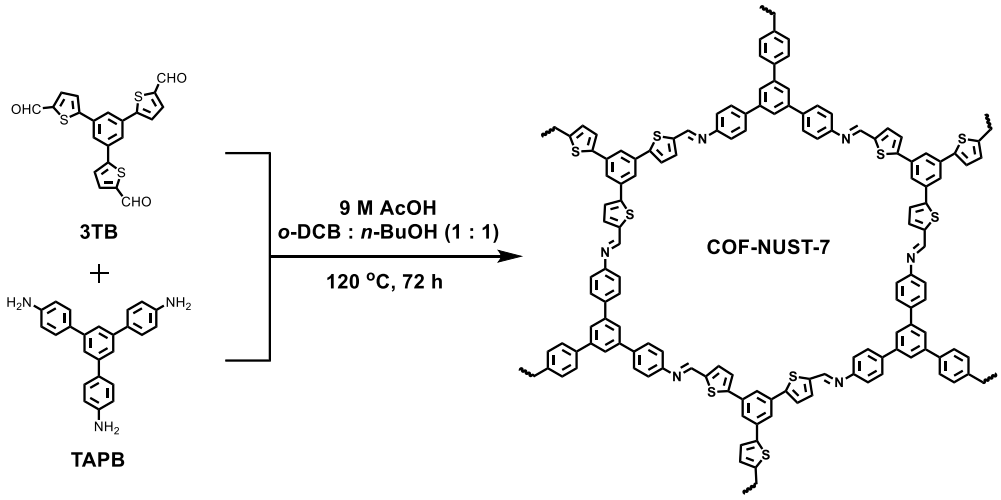

The COF-**NUST-7** powders were synthesized in *o*-DCB and *n*-BuOH with acetic acid as catalyst at 120 °C for three days. In details, **3TB** (20.4 mg, 0.05 mmol), 5'-(4-aminophenyl)-[1,1':3',1"-terphenyl]-4,4"-diamine (**TAPB**, 23.4 mg, 0.05 mmol), *o*-DCB (2 mL), *n*-BuOH (2 mL) and 9 M AcOH (0.2 mL) were charged into a Pyrex tube. Then, the Pyrex tube was ultrasonically treated for around 5 minutes to blend evenly, flash frozen at 77 K, degassed by freeze-pump-thaw three times, and then was sealed. Finally, the reaction mixture was heated at 120 °C for three days. After being cooled to room temperature, the precipitate was isolated by centrifugation and washed with acetone

(3×10 mL) and then filtered. The sample was transferred to vacuum chamber and evacuated to 20 mTorr at 50 °C for 24 h, yielding COF-**NUST-7** as yellow powders.

Synthesis of COF-NUST-8

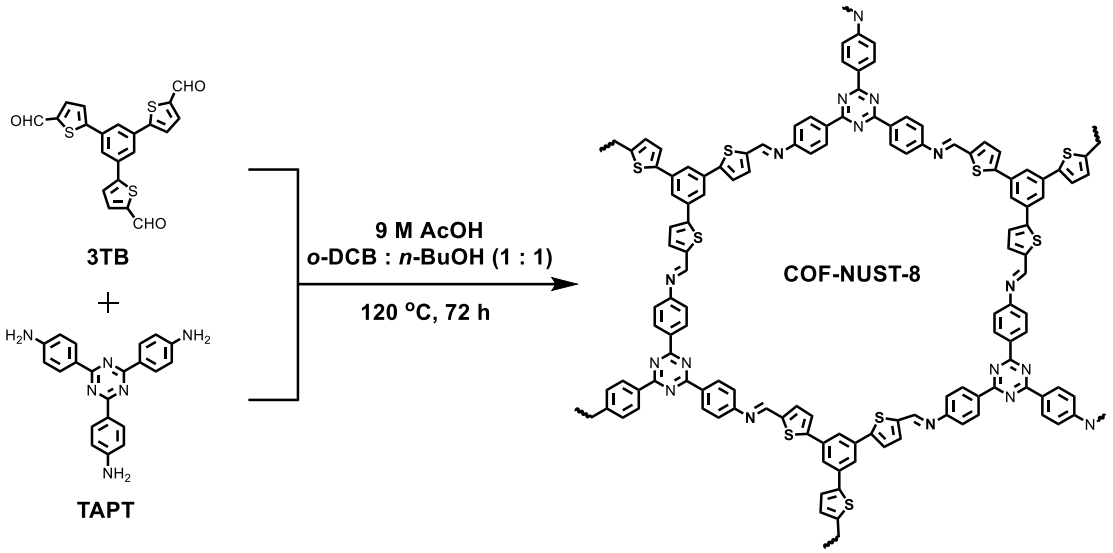

The COF-**NUST-8** powders were synthesized in *o*-DCB and *n*-BuOH with acetic acid as a catalyst at 120 ºC for three days. In details, **3TB** (20.4 mg, 0.05 mmol), 4,4',4"-(1,3,5-triazine-2,4,6-triyl) trianiline (**TAPT**, 17.7 mg, 0.05 mmol), *o*-DCB (2 mL), *n*-BuOH (2 mL) and 9 M AcOH (0.2 mL) were charged into a Pyrex tube. Then, the Pyrex tube was ultrasonically treated for around 5 minutes to blend evenly, flash frozen at 77 K, degassed by freeze-pump-thaw three times, and then was sealed. Finally, the reaction mixture was heated at 120 ºC for three days. After being cooled to room temperature, the precipitate was isolated by centrifugation and washed with acetone (3×10 mL) and then filtered. The sample was transferred to vacuum chamber and evacuated to 20 mTorr at 50 °C for 24 h, yielding COF-**NUST-8** as yellow powders.

Synthesis of COF-NUST-9

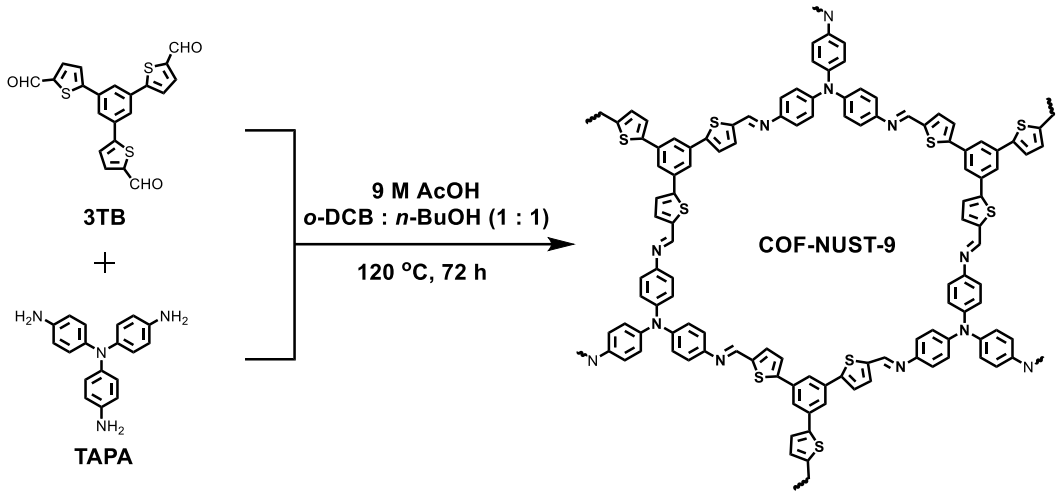

The COF-**NUST-9** were synthesized in *o*-DCB and *n*-BuOH with acetic acid as a catalyst at 120 ºC for three days. In details, **3TB** (20.4 mg, 0.05 mmol), *N,N*-bis(4-aminophenyl)benzene-1,4-diamine (**TAPA**, 14.5 mg, 0.05 mmol), *o*-DCB (2 mL), *n*-BuOH (2 mL) and 9 M AcOH (0.2 mL) were charged into a Pyrex tube. Then, the Pyrex tube was ultrasonically treated for around 5 minutes to blend evenly, flash frozen at 77 K, degassed by freeze-pump-thaw three times, and then was sealed. Finally, the reaction mixture was heated at 120 ºC for three days. After being cooled to room temperature, the precipitate was isolated by centrifugation and washed with acetone (3×10 mL) and then filtered. The sample was transferred to vacuum chamber and evacuated to 20 mTorr at 50 °C for 24 h, yielding COF-**NUST-9** as red powders.

1.3 Preparation of solid composite electrolyte (SCEs)

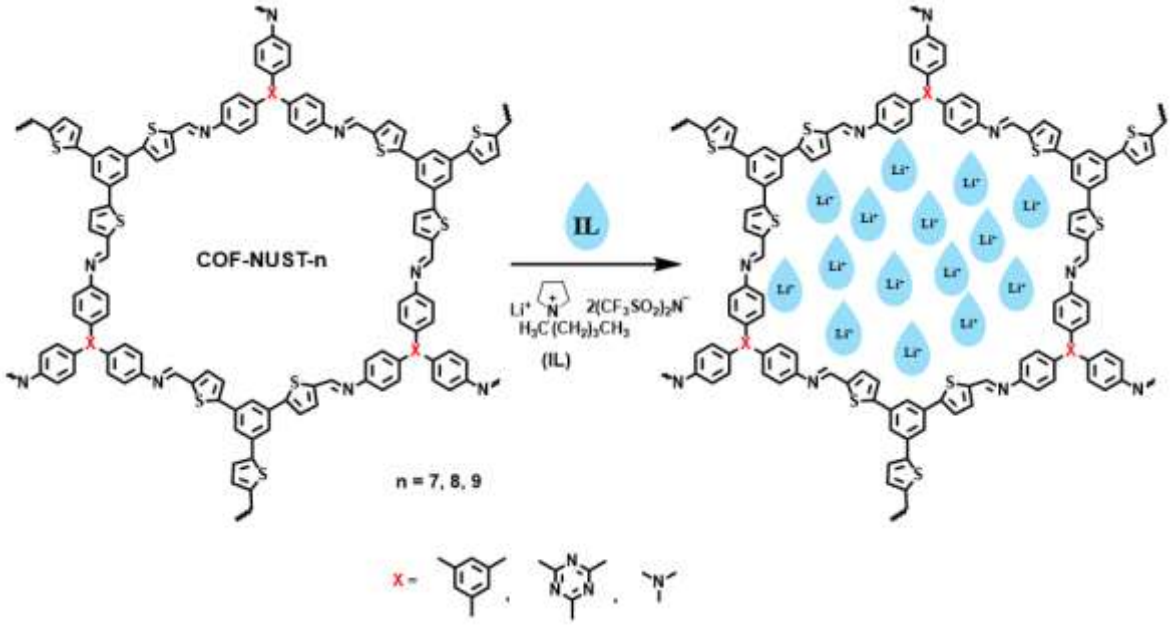

Solid composite electrolytes (SCEs) were prepared by pressing pellets for electrochemical tests. The COFs powers were dried at 100 ºC under vacuum for 12 h. Then, the powders were dried on a hotplate at 110 ºC in a glovebox for three days before use to exclude possible water or solvents influence. SCEs powders were prepared by doping ionic liquids (IL) and lithium salts (LiTFSI) into COFs powders. Firstly, LiTFSI was dissolved in ionic liquids (IL) at certain weight ratios (1/2, 1/4, and 1/8). Then COFs powders and IL/LiTFSI solutions were grinded for ten minutes. IL/LiTFSI could be easily doped into COFs powders channels due to its high porosity. Finally, the mixtures (ca. 6-10 mg) were pressed into pellets at 2 T for 20 minutes by a standard 5 mm die. All the pellets preparation processes were in an Ar atmosphere glovebox with O_2 and H_2O less than 0.5 ppm.

1.4 Ionic conductivities testing

The SCEs pellets were sandwiched between two stainless steel electrodes, assembled in coin cells in glovebox. Ionic conductivities were evaluated and collected in a temperature range from 40 to 120 ºC with an increment of 10 ºC. The coin cells were tested at a frequency range from 7 MHz to 0.1 Hz with an amplitude voltage of 10 mV by a Biological SP-200 portable working station.

1.5 Electrochemical performance tests of solid lithium battery

Composite cathode was prepared by importing IL and LiTFSI to provide smooth ionic pathways. $LiFePO_4$ powders, carbon black, PVDF, and (IL+LiTFSI) were mixed in a weight ratio of 8:1:1:2. IL and LiTFSI were mixed and dissolved in a weight ratio of 4 in glovebox in advance. After stirring in NMP for 12 h, the slurry was casted onto an aluminum foil, and then were dried in a Compact Tape Casting Coater at 110 ^{o}C for 40 minutes. Then the foil was punched into small discs. Polyethylene oxide (PEO, Mw=600, 000)-LiTFSI electrolytes were prepared as contrast group. PEO and LiTFSI were first mixed at a [EO]/[Li] molar ratio of 8, and dissolved in acetonitrile (AN). After stirring at 65 ^{o}C for 4 h, the solution was casted into a PTFE mold, and dried at 60 ^{o}C for 48 h to evaporate the solvent in a vacuum oven. Then the PEO-LiTFSI electrolyte film was transferred and dried on a hotplate of 50 ^{o}C in a glovebox for three days before use. PEO-LiTFSI film was peeled off and punched into small discs, assembling into solid lithium coin cell with composite $LiFePO_4$ cathode and lithium foil. All solid lithium full cells were assembled in a glovebox with O_2 and H_2O less than 0.5 ppm. All cells were tested between 2.5 and 3.8 V at 0.05 C at 100 ^{o}C.

2 Characterization Section

2.1 Fourier transform infrared (FTIR) spectra of COFs

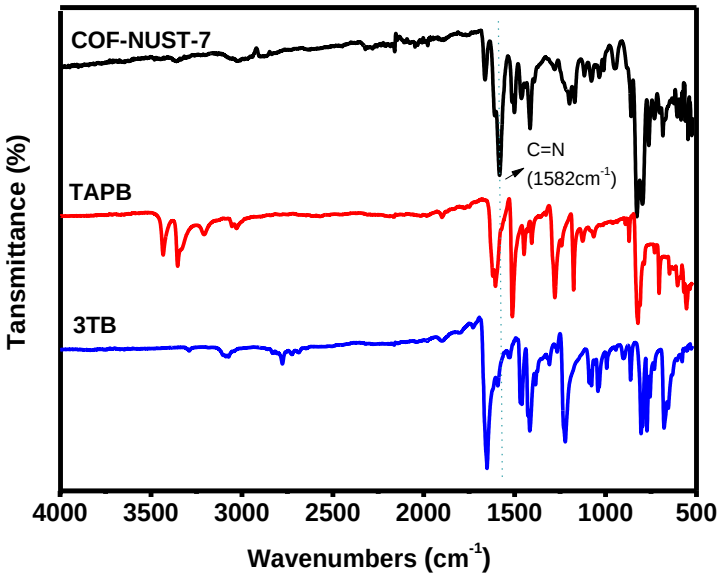

Figure S2. FTIR spectra of **3TB**, **TAPB**, and COF-**NUST-7**

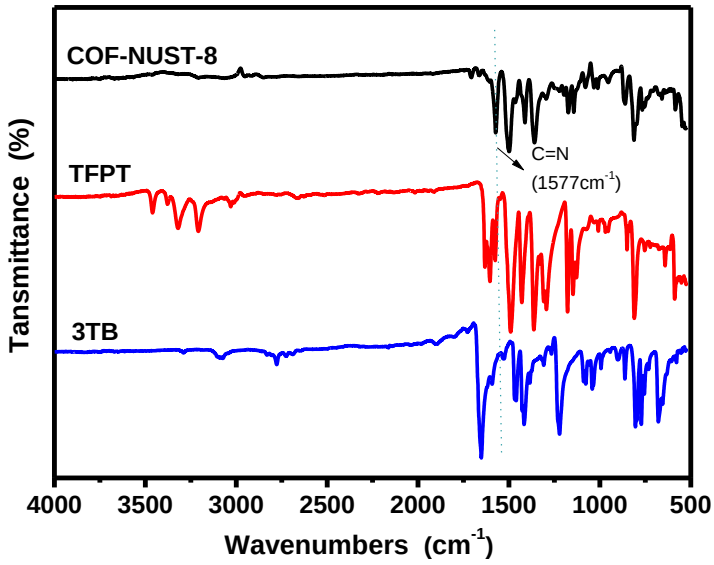

Figure S3. FTIR spectra of **3TB**, **TAPT**, and COF-**NUST-8**

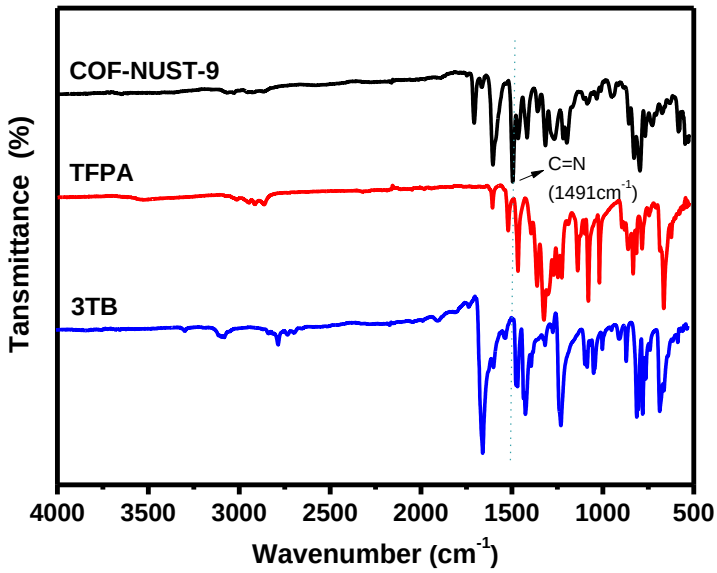

Figure S4. FTIR spectra of **3TB**, **TAPA**, and COF-**NUST-9**

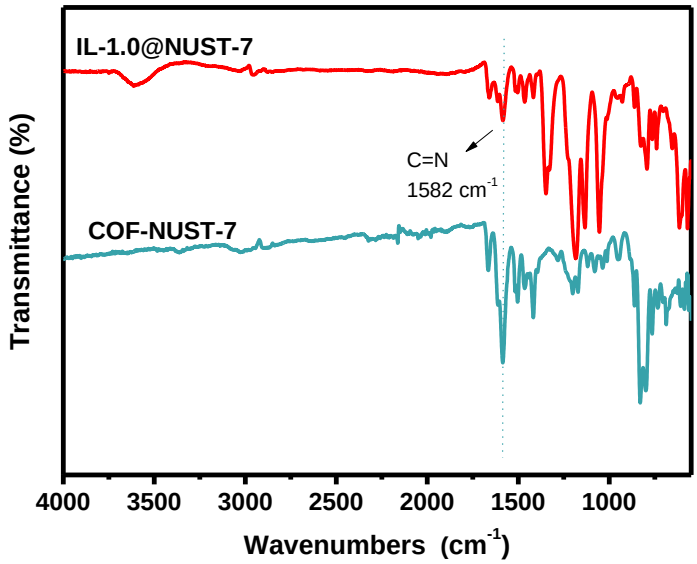

Figure S5. FTIR spectra of COF-**NUST-7** and IL-1.0@**NUST-7** powders

2.2 ^{13}C CPMAS NMR spectra of COFs

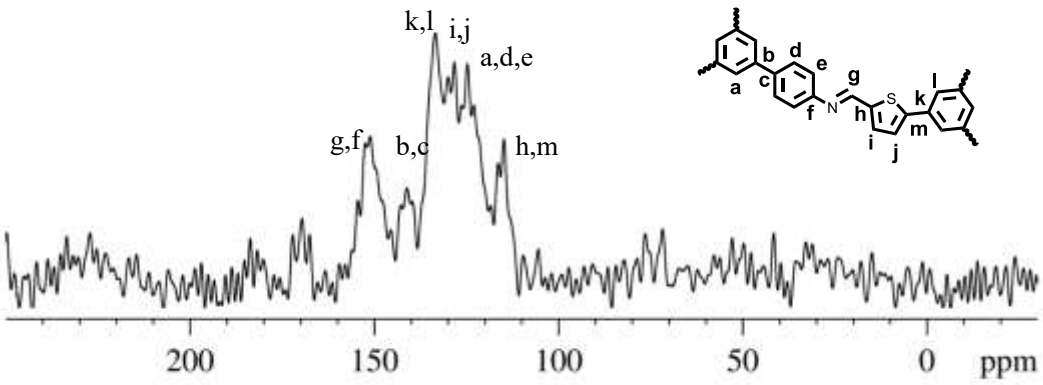

Figure S6. ^{13}C NMR spectra of COF-**NUST-7** powders

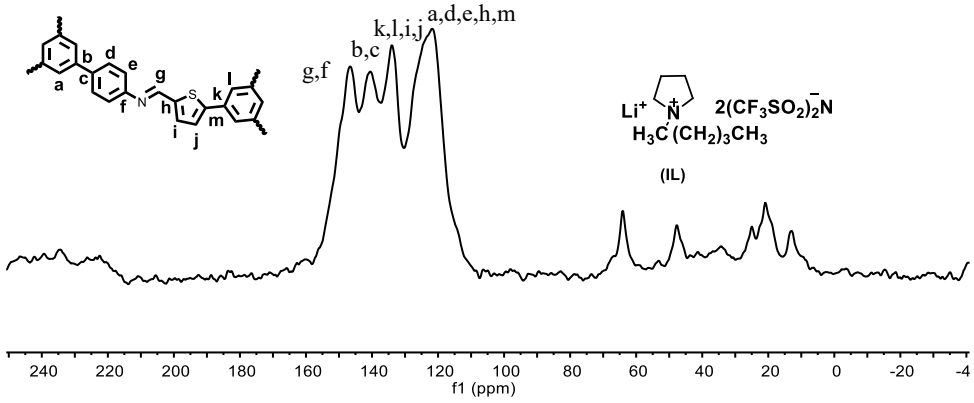

Figure S7. ^{13}C NMR spectra of IL-1.0@COF-**NUST-7** powders.

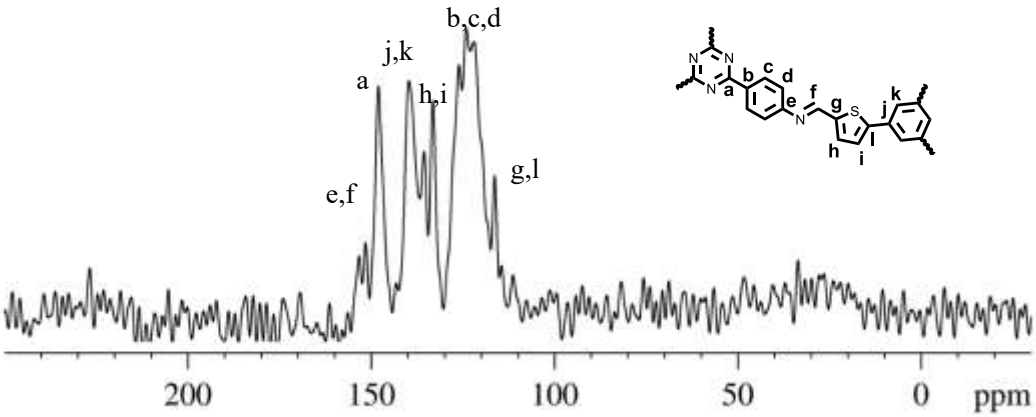

Figure S8. ^{13}C NMR spectra of COF-**NUST-8** powders

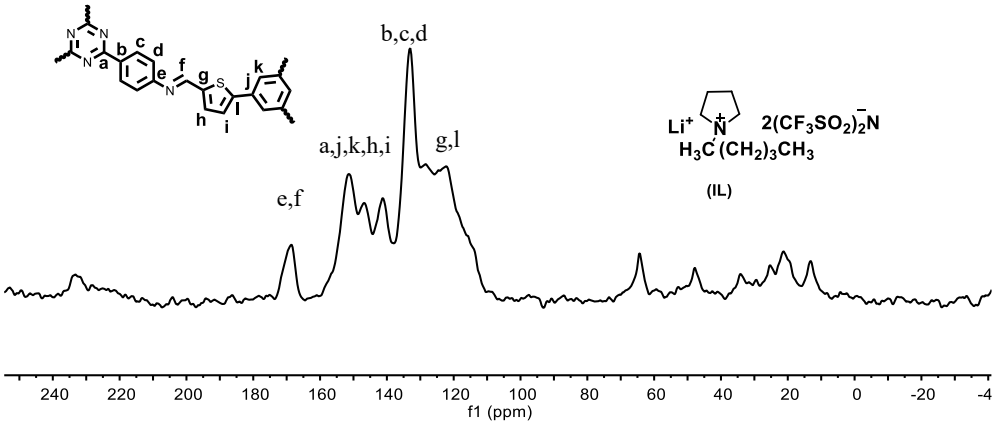

Figure S9. ^{13}C NMR spectra of IL-1.0@COF-**NUST-8** powders.

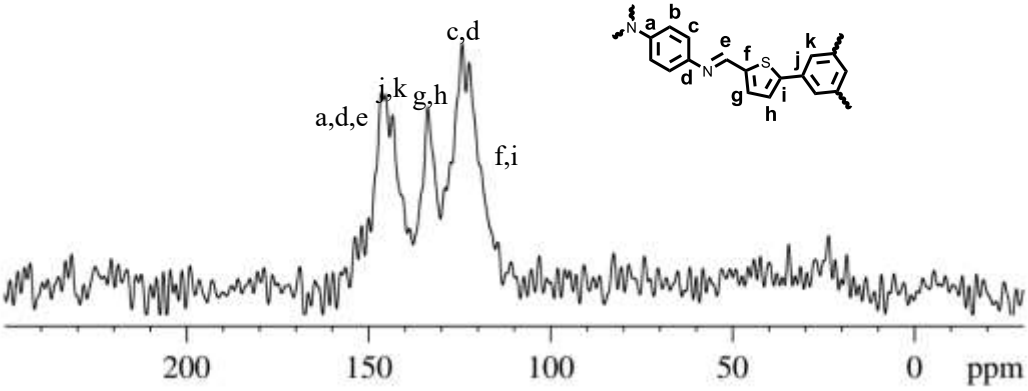

Figure S10. ^{13}C NMR spectra of COF-**NUST-9** powders

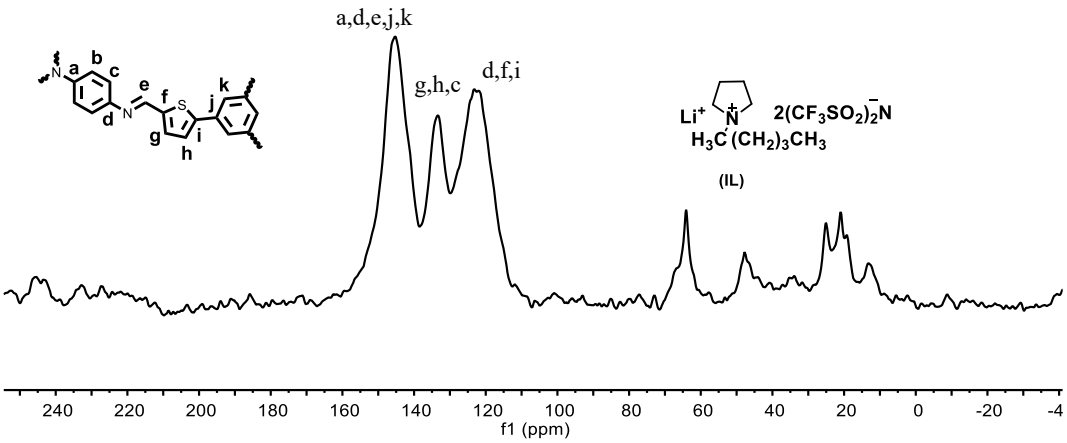

Figure 11. ^{13}C NMR spectra of IL-1.0@COF-**NUST-9** powders.

2.3 Scanning electron microscopy (SEM) images of COFs

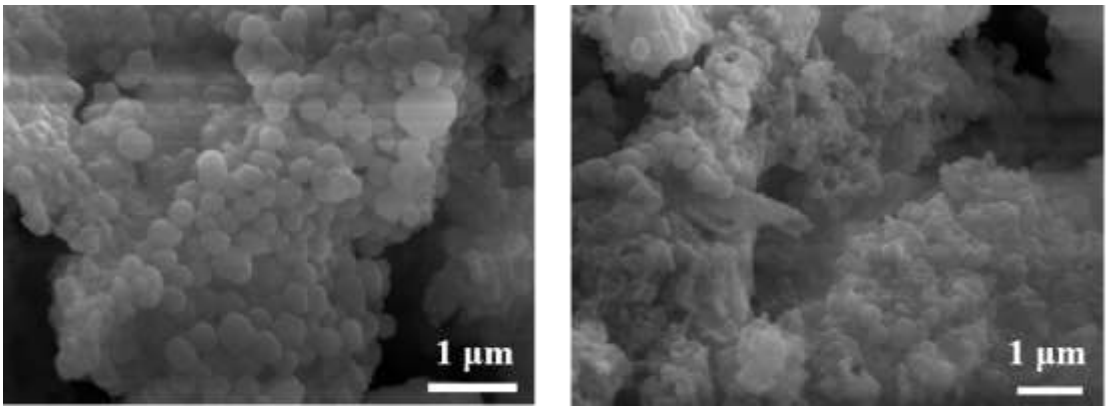

Figure S12. SEM images of COF-**NUST-7** powders

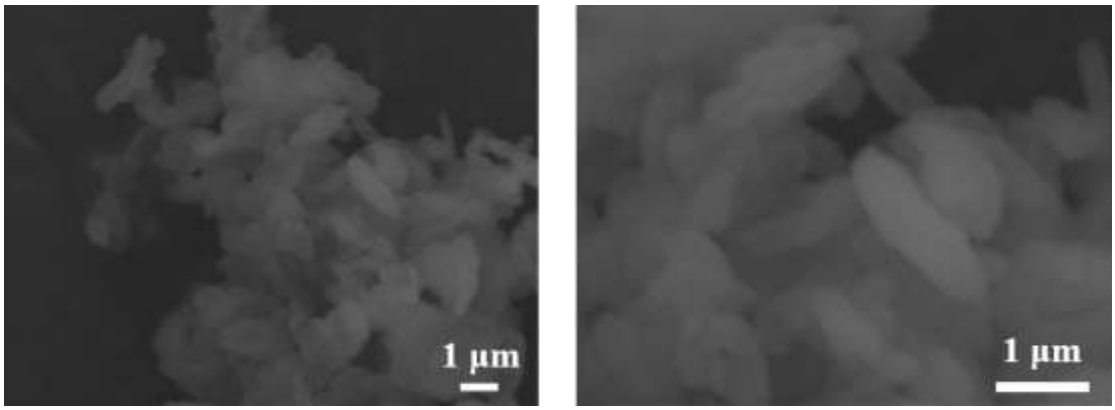

Figure S13. SEM images of COF-**NUST-8** powders

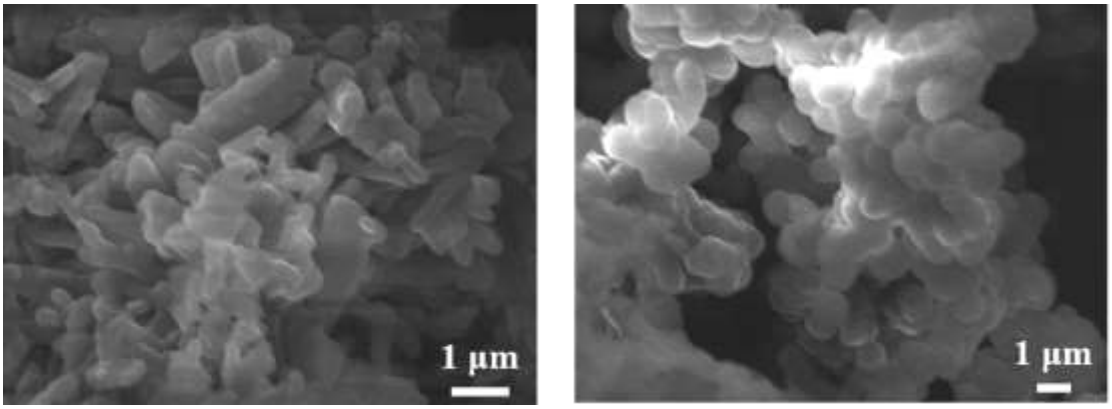

Figure S14. SEM images of COF-**NUST-9** powders

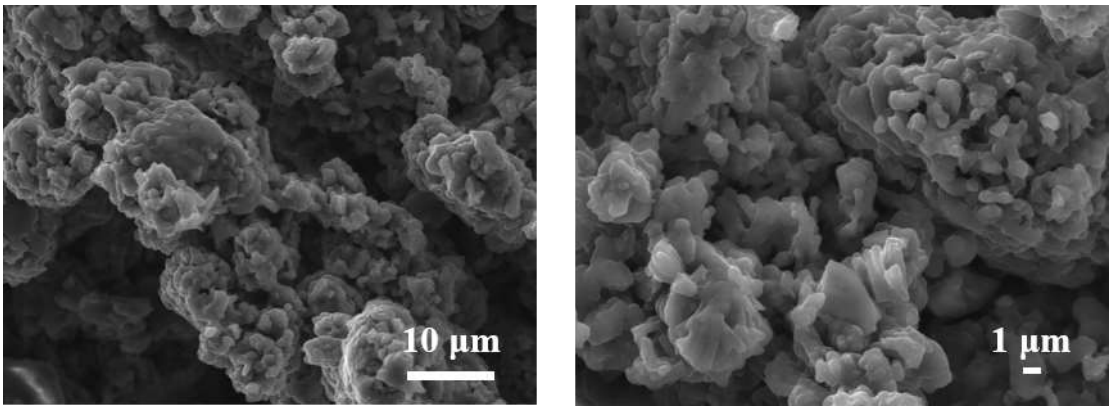

Figure S15. SEM images of IL-1.0@**NUST-7** powders

2.4 Transmission electron microscopy (TEM) images of COFs

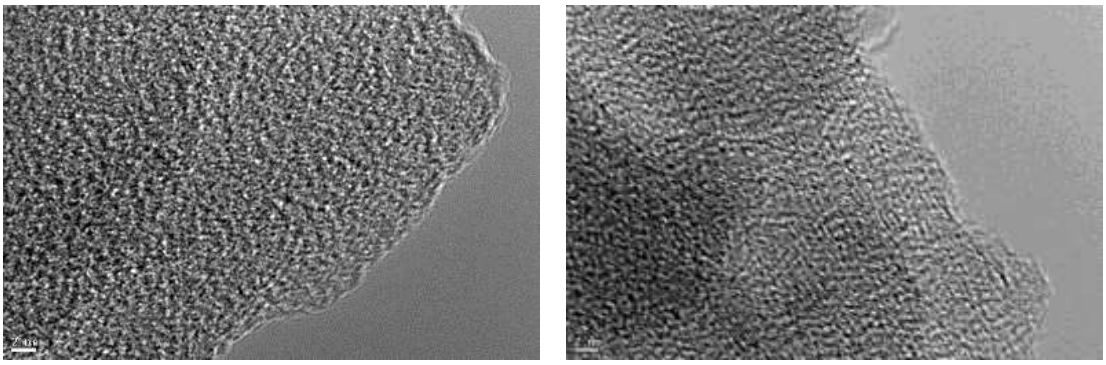

Figure S16. TEM images of COF-**NUST-7** powders

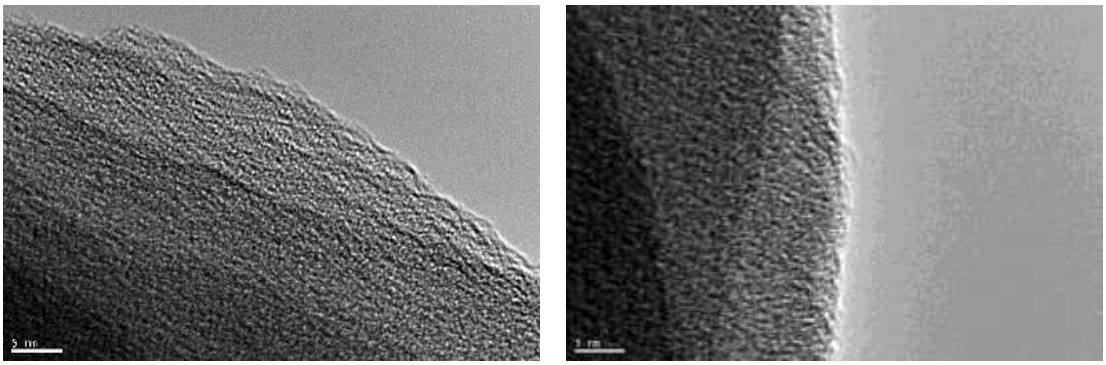

Figure S17. TEM images of COF-**NUST-8** powders

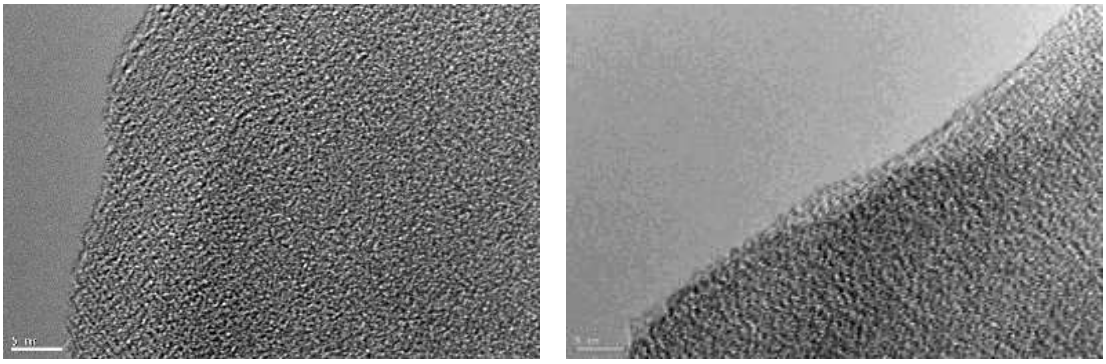

Figure S18. TEM images of COF-**NUST-9** powders

2.5 Thermogravimetric analysis (TGA) of COFs

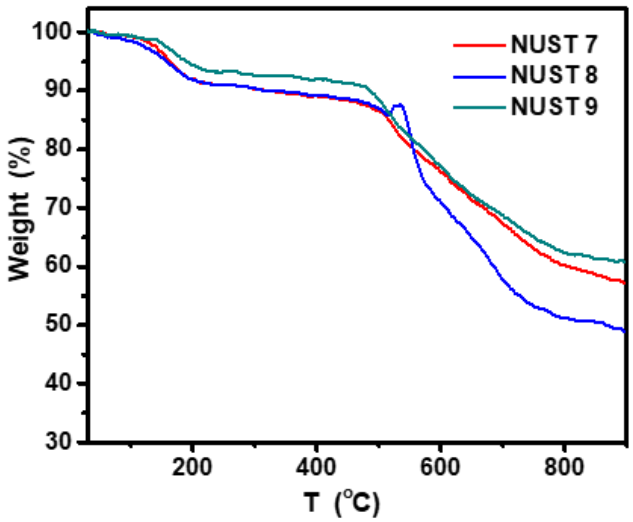

Figure S19. TGA curves of COFs powders

2.6 N_2 adsorption-desorption isotherms and pore size distribution of COFs

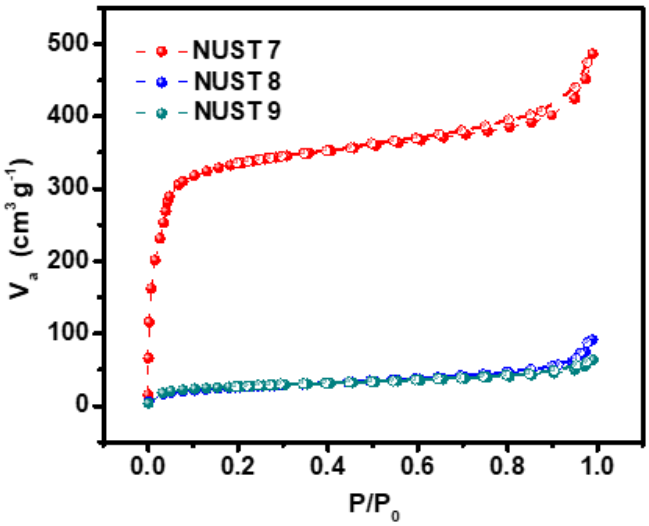

Figure S20. N_2 adsorption-desorption isotherms at 77 K of COFs powders

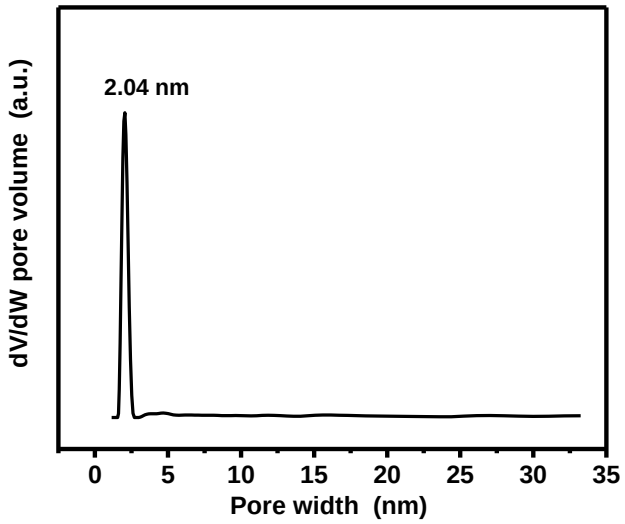

Figure S21. PSD of calculated of COF-**NUST-7** from N_2 sorption (slit/cylinder, QSDFT adsorption branch).

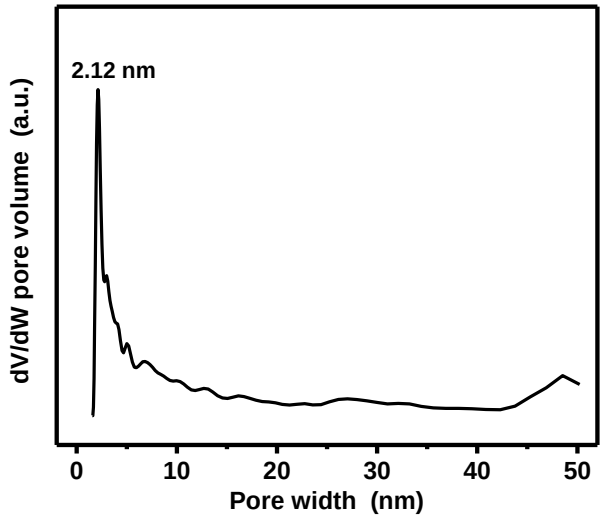

Figure S22. PSD of calculated of COF-**NUST-8** from N_2 sorption (slit/cylinder, QSDFT adsorption branch).

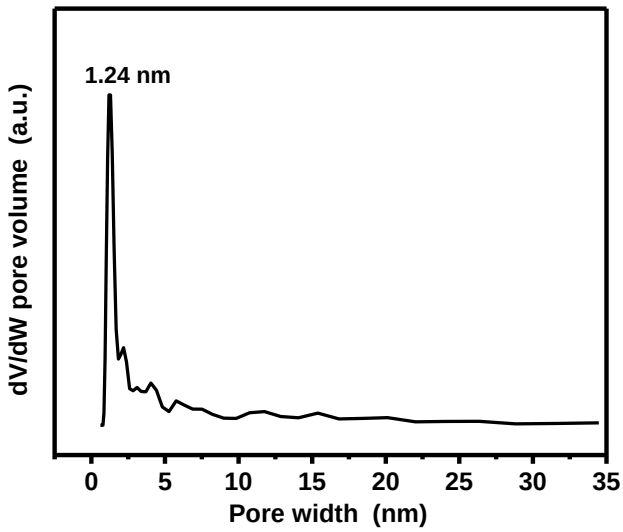

Figure S23. PSD of calculated of COF-**NUST-9** from N_2 sorption (slit/cylinder, QSDFT adsorption branch).

2.7 Powder X ray diffraction (PXRD), structure modeling, and atomic coordinates of COFs

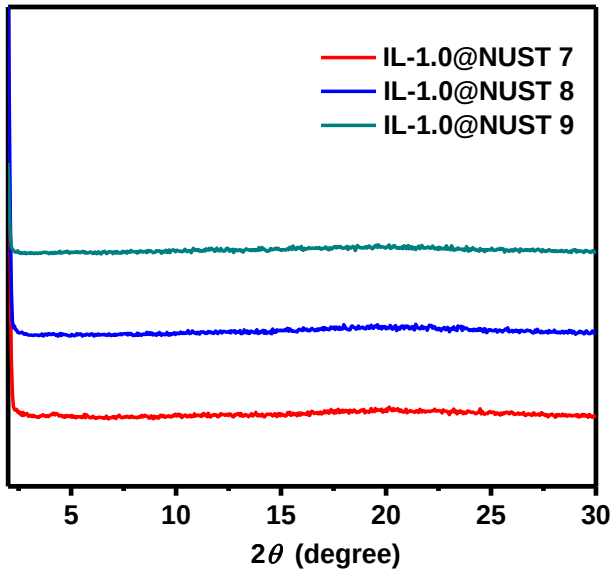

Figure S24. PXRD patterns of COFs after doping with IL and LiTFSI.

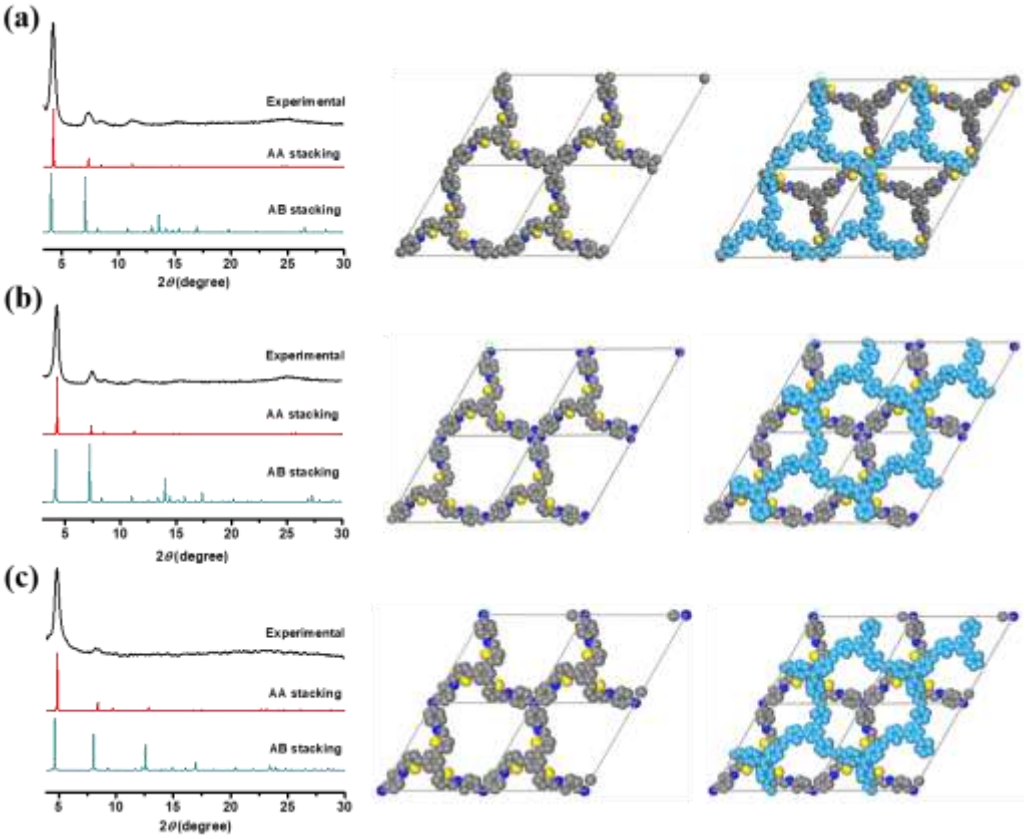

Figure S25. Simulated PXRD patterns and Top views for AA and AB structure of **(a)** COF-**NUST-7**; **(b)** COF-**NUST-8**; **(c)** COF-**NUST-9**.

Table S1. Fractional atomic coordinates for simulated COF-**NUST-7** powders

Space group: *P3*			
3D hexagonal; a = b = 23.59 Å, c = 3.43 Å; α = β = 90°, γ = 120°			
Atom	x	y	z
C1	0.13497	0.08281	-0.09579
C2	0.17571	0.06385	-0.24154
C3	0.24035	0.10288	-0.22218
C4	0.26624	0.16249	-0.06836
C5	0.22612	0.18227	0.07421
C6	0.16148	0.14274	0.06338
N7	0.33308	0.19993	-0.04902
C8	0.36519	0.25886	0.0323
C9	0.43348	0.29014	0.05409
C10	0.0656	0.04026	-0.10435
C11	0.02495	0.06458	-0.10531
S12	0.47481	0.25278	-0.02364
C13	0.54235	0.32141	0.07162
C14	0.53186	0.3699	0.16008
C15	0.46981	0.35197	0.14875
C16	0.60515	0.32704	0.06583
C17	0.61096	0.27359	0.06315
H18	0.15533	0.01429	-0.38271
H19	0.27385	0.08553	-0.33694
H20	0.24699	0.23267	0.2045
H21	0.12893	0.16031	0.19059
H22	0.33942	0.2874	0.08891
H23	0.04538	0.11917	-0.10696
H24	0.57433	0.41969	0.23364
H25	0.44629	0.38254	0.20853
H26	0.56584	0.22356	0.05865

Table S2. Fractional atomic coordinates for simulated COF-**NUST-8** powders

Space group: *P3*			
3D hexagonal; a = b = 24.43 Å, c = 3.23 Å; α = β = 90°, γ = 120°			
Atom	x	y	z
C1	0.13728	0.08954	-0.40381
C2	0.18264	0.06694	-0.41815
C3	0.24792	0.10782	-0.31927
C4	0.26905	0.1716	-0.2021
C5	0.22493	0.1959	-0.20685
C6	0.15963	0.15513	-0.30719
N7	0.3349	0.20874	-0.07351
C8	0.35982	0.26314	0.09707
C9	0.42777	0.29281	0.21829
C10	0.06616	0.04324	-0.45482
N11	0.02275	0.06565	-0.45335
S12	0.47426	0.25589	0.16474
C13	0.5382	0.32187	0.36193
C14	0.52299	0.36913	0.46576
C15	0.45964	0.35228	0.38389
C16	0.60394	0.32789	0.39845
C17	0.60991	0.27116	0.40088
H18	0.16726	0.01697	-0.49542
H19	0.28171	0.08891	-0.32229
H20	0.23983	0.24558	-0.12898
H21	0.12609	0.17429	-0.29594
H22	0.33117	0.28617	0.16083
H23	0.55624	0.41387	0.59869
H24	0.43771	0.38227	0.44222
H25	0.56597	0.22308	0.39096

Table S3. Fractional atomic coordinates for simulated COF-**NUST-9** powders

Space group: *P3*			
3D hexagonal; a = b = 20.18 Å, c = 3.80 Å; α = β = 90°, γ = 120°			
Atom	x	y	z
C1	0.07984	0.04448	-0.22008
C2	0.12135	0.01897	-0.04591
C3	0.19566	0.06392	0.0126
C4	0.23041	0.13687	-0.08578
C5	0.19181	0.16303	-0.27431
C6	0.11804	0.11658	-0.34928
N7	0.30374	0.18294	0.02692
C8	0.33345	0.25166	0.10236
C9	0.40711	0.28823	0.2465
S10	0.45645	0.24479	0.27612
C11	0.5257	0.32166	0.46246
C12	0.50964	0.37733	0.50246
C13	0.44158	0.358	0.37806
C14	0.59745	0.3279	0.53601
C15	0.60361	0.26478	0.54345
H16	0.09715	-0.03516	0.05514
H17	0.22529	0.04301	0.15616
H18	0.21818	0.21916	-0.36099
H19	0.09016	0.1395	-0.48518
H20	0.30291	0.28016	0.08643
H21	0.54544	0.42999	0.61761
H22	0.4181	0.39322	0.38466
H23	0.55487	0.21182	0.52933
N24	1	1	-0.243

3 Electrochemical Performance

Table S4. Corresponding abbreviations for each material in paper

	Abbreviations		**Sample**	
COF-NUST-7	COF-**NUST 7**-2	Adjust the ratio of IL/LiTFSI	(IL+LiTFSI)/COFs=1.0	IL/LiTSFI=2/1
	COF-**NUST 7**-8			IL/LiTSFI=8/1
	IL-1.0@**NUST-7**			IL/LiTSFI=4/1
	IL-0.75@**NUST-7**	Adjust the ratio of (IL+LiTFSI)/COFs	(IL+LiTFSI)/COFs=0.75	IL/LiTSFI=4/1
	IL-0.5@**NUST-7**		(IL+LiTFSI)/COFs=0.5	
	IL-0.25@**NUST-7**		(IL+LiTFSI)/COFs=0.25	
COF-NUST-8	IL-1.0@**NUST-8**	Based on the optimized ratio from **NUST-7** sample	(IL+LiTFSI)/COFs=1.0	IL/LiTSFI=4/1
COF-NUST-9	IL-1.0@**NUST-9**		(IL+LiTFSI)/COFs=1.0	IL/LiTSFI=4/1

3.1 Ionic conductivity tests

Table S5. The activation energies of IL-1.0@**NUST-7**, COF-**NUST 7**-8 and COF-**NUST 7**-2

	IL-1.0@**NUST-7**	COF-**NUST 7**-8	COF-**NUST 7**-2
Ea (eV)	0.317	0.273	0.395

Table S6. The activation energies of IL-0.25@**NUST-7**, IL-0.5@**NUST-7**, IL-0.75@**NUST-7**, and IL-1.0@**NUST-7**

	IL-0.25@**NUST-7**	IL-0.5@**NUST-7**	IL-0.75@**NUST-7**	IL-1.0@**NUST-7**
Ea (eV)	0.302	0.305	0.306	0.317

Table S7. The activation energies of IL-1.0@**NUST-7**, IL-1.0@**NUST-8** and IL-1.0@**NUST-9**

	IL-1.0@**NUST-7**	IL-1.0@**NUST-8**	IL-1.0@**NUST-9**
Ea (eV)	0.317	0.301	0.323

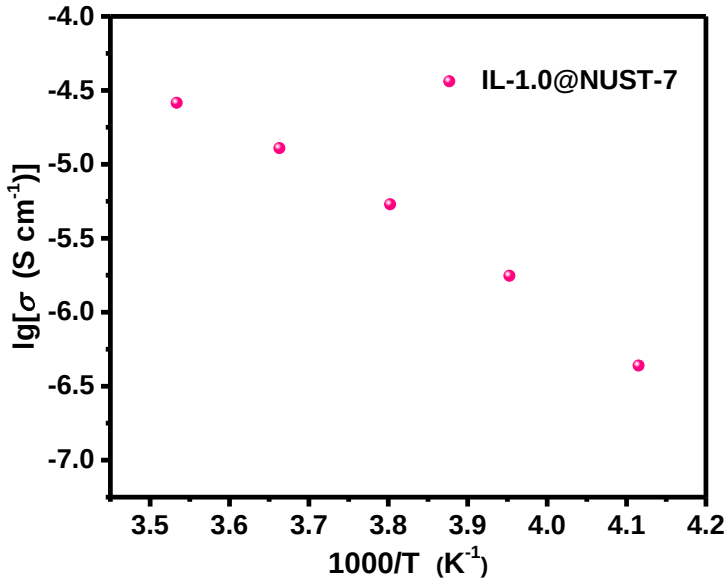

Figure S26. Temperature-dependent Li^+ conductivities of IL-1.0@**NUST-7** from -30 ºC to 10 ºC.

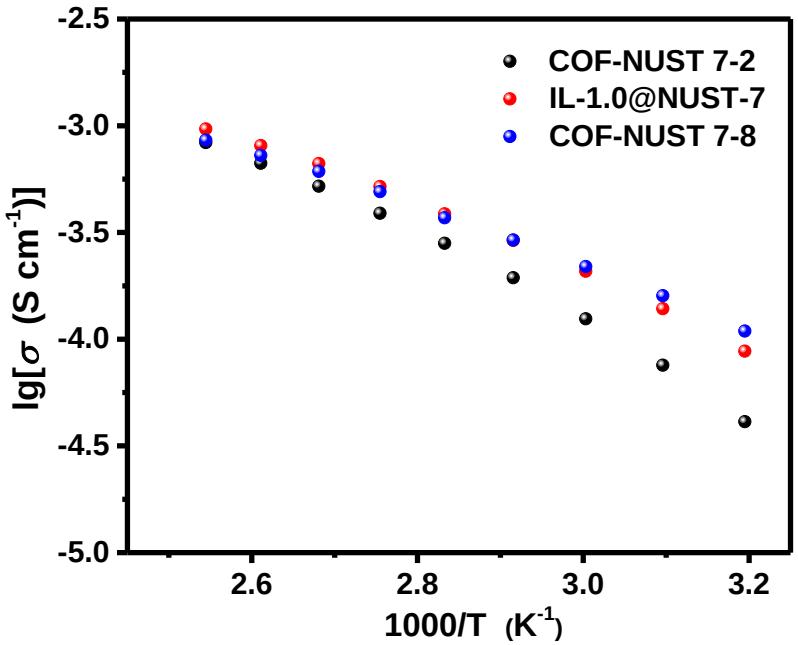

Figure S27. A Temperature-dependent Li^+ conductivities of COF-**NUST 7**-2, IL-1.0@**NUST-7**, COF-**NUST 7**-8 from 40 ºC to 120 ºC.

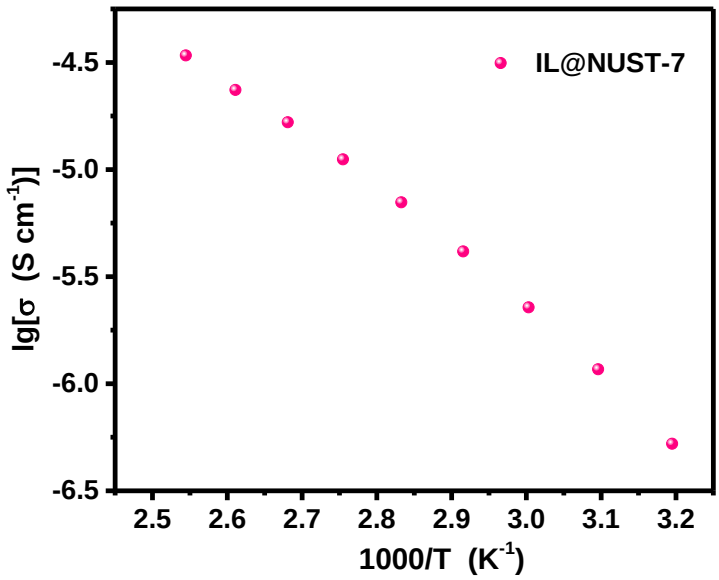

Figure S28. Temperature-dependent Li^+ conductivities of COF-**NUST-7** doping with only ionic liquid at a weight ratio of 1/1.

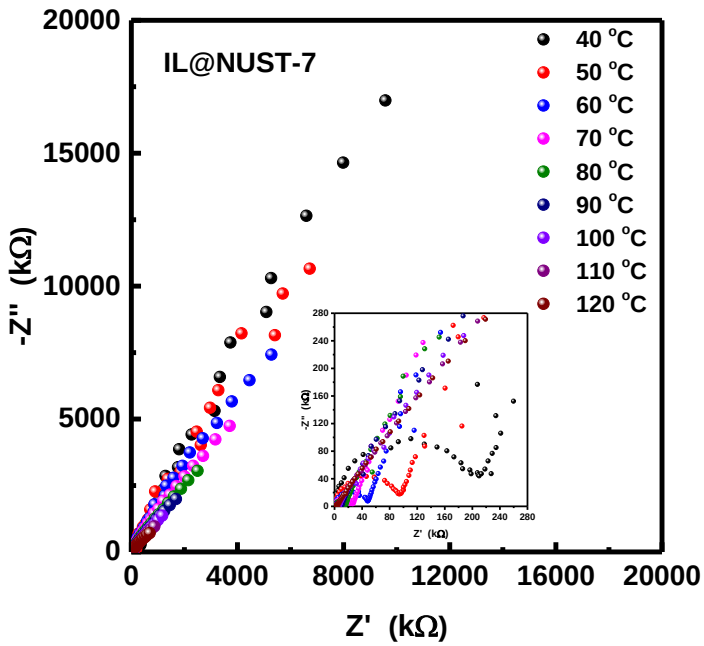

Figure S29. Nyquist plots of COF-**NUST-7** doping with only ionic liquid at a weight ratio of 1/1 at different temperatures.

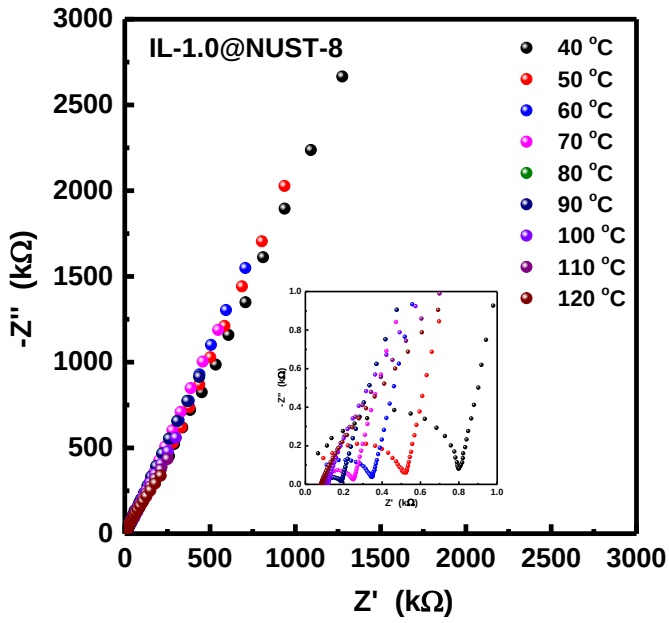

Figure S30. Nyquist plots of IL-1.0@**NUST-8**.

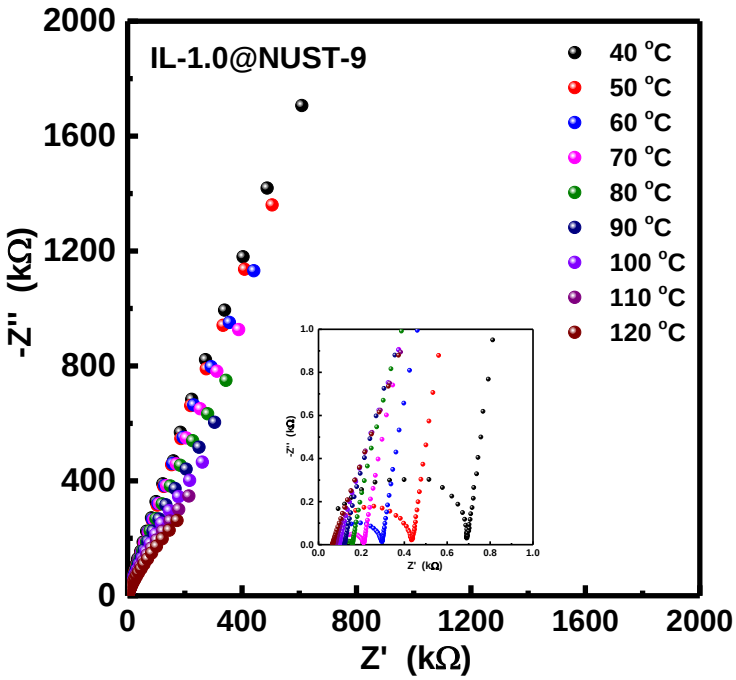

Figure S31. Nyquist plots of IL-1.0@**NUST-9**.

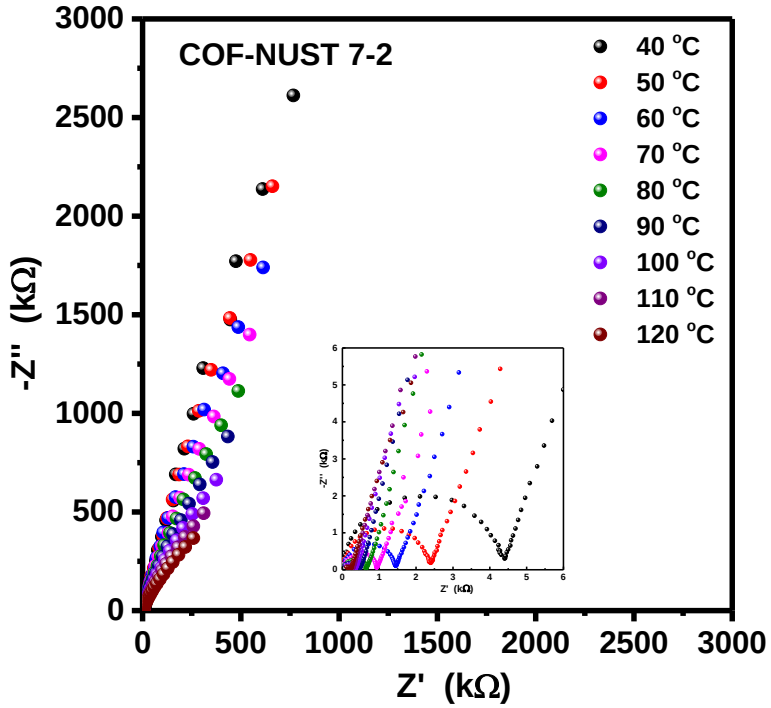

Figure S32. Nyquist plots of COF-**NUST 7**-2.

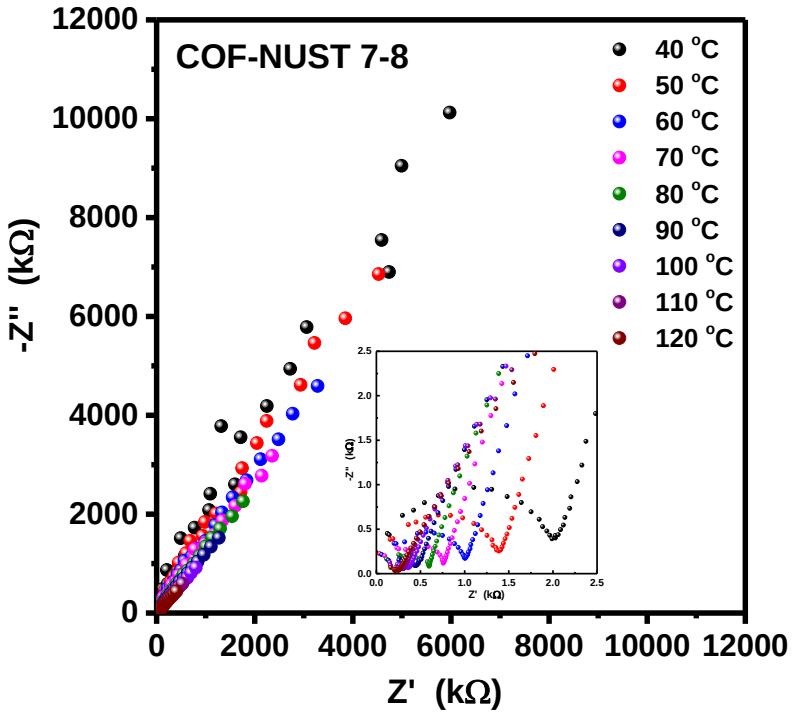

Figure S33. Nyquist plots of COF-**NUST 7**-8.

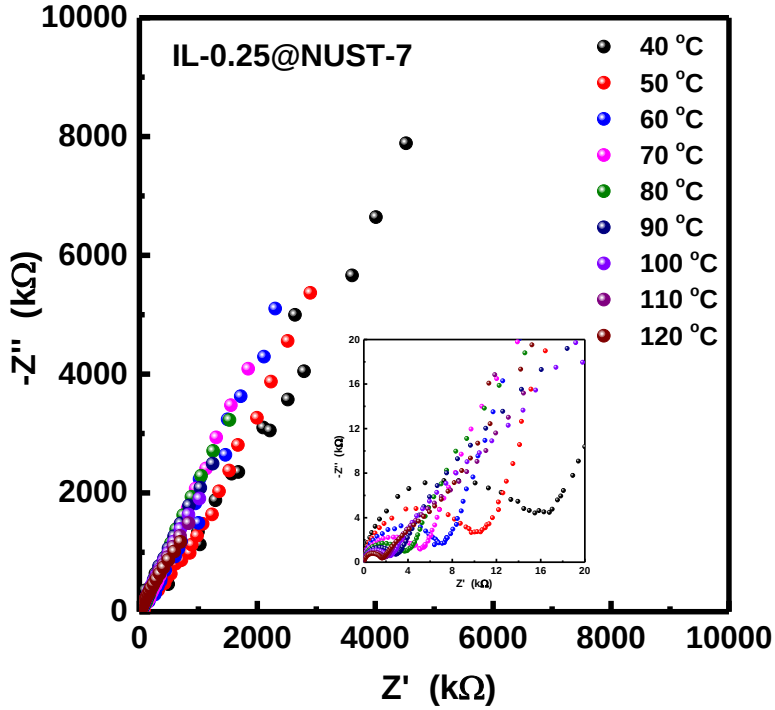

Figure S34. Nyquist plots of IL-0.25@**NUST-7**.

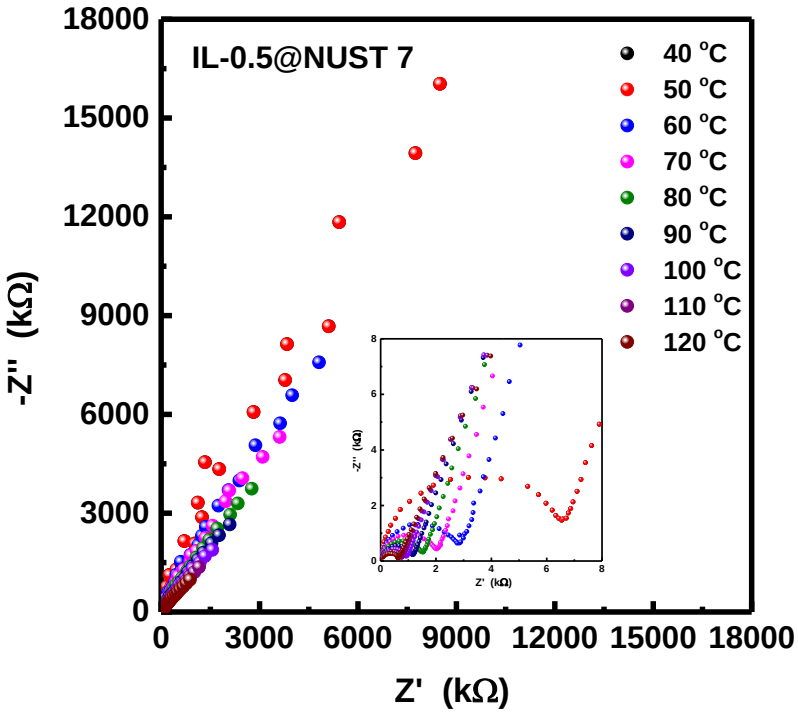

Figure S35. Nyquist plots of IL-0.5@**NUST-7**.

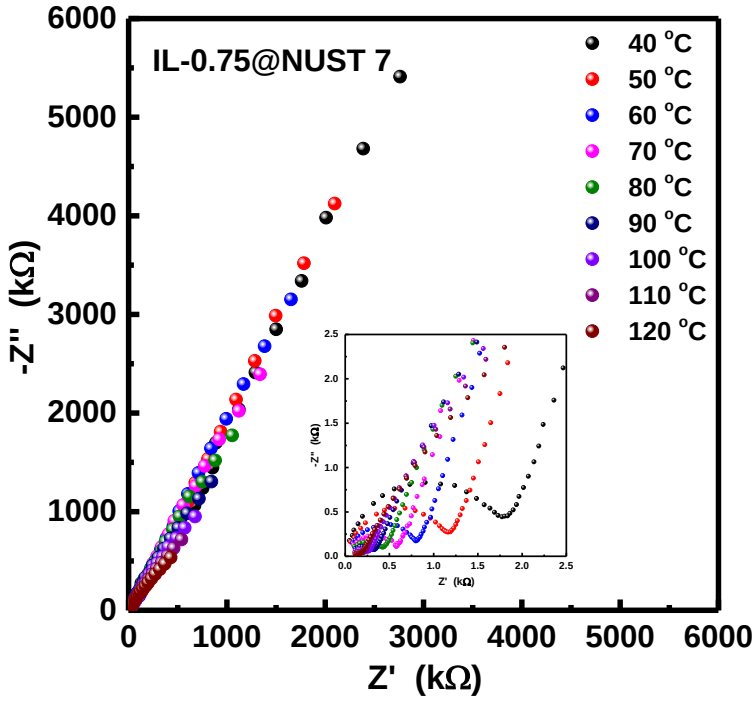

Figure S36. Nyquist plots of IL-0.75@**NUST-7**.

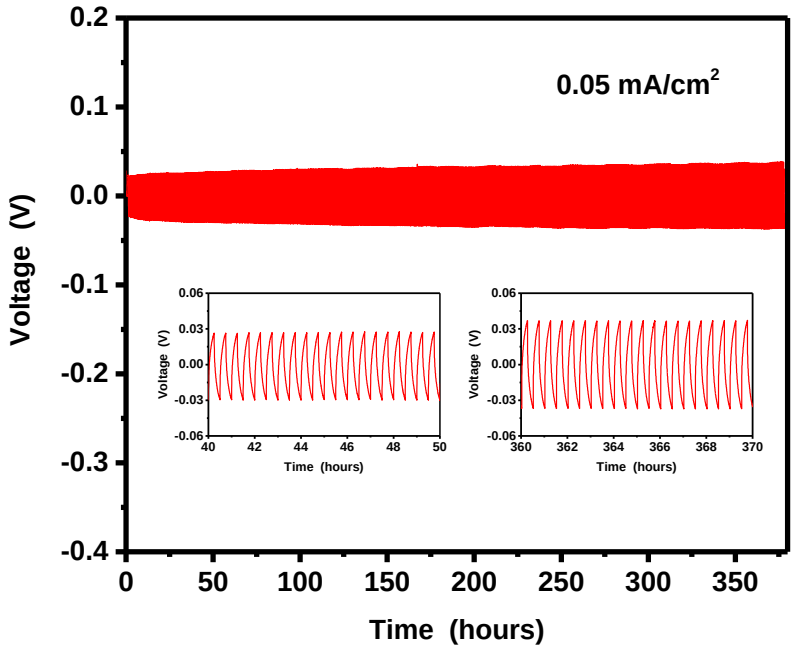

Figure S37. Electrochemical characterizations of the IL-1.0@**NUST-7** electrolyte in Li/Li symmetric cells at 100 ºC.

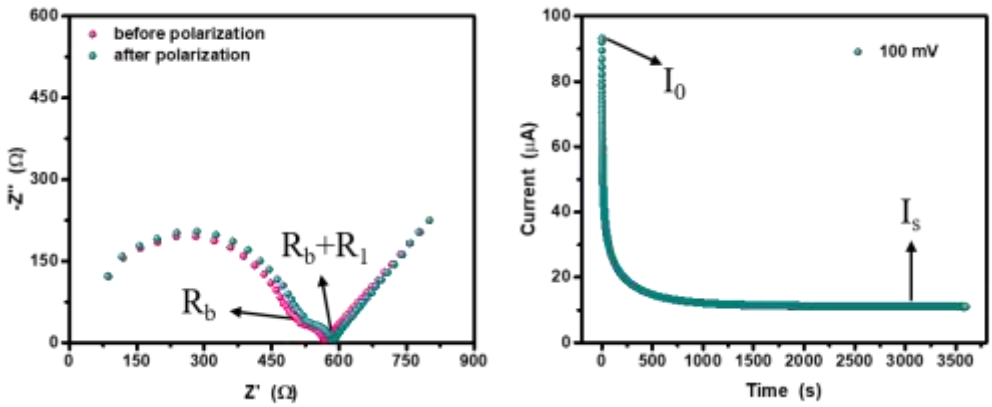

Figure S38. Electrochemical impedance spectra before and after polarization at 100 mV and the corresponding polarization curves

Measurements of Li^+ transference number (t_{Li+}): Li^+ transference number were evaluated in a Li/COFs electrolyte/Li system by a potentiostatic polarization method.[3, 4] A CA polarization with the potential of 100 mV was applied until the current reached a steady state. The Li^+ transference number could be calculated from equation 1:

$$t_{Li^+} = \frac{I_s R_b^0 [\Delta V - I_0 \ R_1^0]}{I_0 R_b^s [\Delta V - I_s \ R_1^s]} \qquad \textbf{(eq.1)}$$

where t_{Li+} is the Li^+ transference number, ΔV is polarization voltage, I_0 and I_s are initial current and steady-state current obtained by constant voltage polarization method testing, R_b^0 and R_b^s are the intrinsic resistance of the electrolyte before and after the test, R_1^0 and R_1^s are the interface resistance before and after the test, respectively. Hence, the t_{Li+} was 0.11.

3.2 Li^+ conductivity comparison between this work and literatures

Table S8. Li^+ conductivity comparison between this work and literatures

	Materials	Conductivity (mS cm^{-1})	Reference
1	CD-COF-Li⊃$LiPF_6$-EC-DMC	2.7 (EC-DMC, 30 °C)	Ref. 5
2	H-Li-ImCOF	5.3 (PC, RT)	Ref. 6
3	DBC-2P⊂PEG-28 wt%	0.045 (70 °C)	Ref. 7
4	PEG-Li^+@EB-COF-ClO_4	1.78 (120 °C)	Ref. 8
5	TpPa-SO_3Li	0.027 (PC, RT)	Ref. 9
6	COF-PEO-9-LiTFSI	0.12 (100 °C)	Ref. 10
7	IL-1.0@NUST-9	2.6 (120 °C)	**This work**

Reference

1. Dong, Y.; Luo, F.; Chen, L.; Yuan, F.; Hou, Y.; Li, W.; Yan, S.; Dai, Y.; Ouyang, M.; Zhang, C., Multi-color

electrochromism containing green color based on electrochemically polymerized star-shaped phenyl bithiophene. *Phys. Chem. Chem. Phys.,* **2018,** *20* (18), 12923-12928.

2. Kotha, S.; Todeti, S.; Gopal, M. B.; Datta, A., Synthesis and Photophysical Properties of C3-Symmetric Star-Shaped Molecules Containing Heterocycles Such as Furan, Thiophene, and Oxazole. *ACS Omega.* **2017,** *2* (10), 6291-6297.
3. Zhou, N.; Wang, Y.; Zhou, Y.; Shen, J.; Zhou, Y.; Yang, Y., Star-shaped multi-arm polymeric ionic liquid based on tetraalkylammonium cation as high performance gel electrolyte for lithium metal batteries. *Electrochimica Acta,* **2019,** *301*, 284-293.
4. Zhou, Y.; Yang, Y.; Zhou, N.; Li, R.; Zhou, Y.; Yan, W., Four-armed branching and thermally integrated imidazolium-based polymerized ionic liquid as an all-solid-state polymer electrolyte for lithium metal battery. *Electrochimica Acta,* **2019,** *324*, 134827.
5. Zhang, Y.; Duan, J.; Ma, D.; Li, P.; Li, S.; Li, H.; Zhou, J.; Ma, X.; Feng, X.; Wang, B., Three-Dimensional Anionic Cyclodextrin-Based Covalent Organic Frameworks. *Angew. Chem. Int. Ed.* **2017,** *56* (51), 16313-16317.
6. Hu, Y.; Dunlap, N.; Wan, S.; Lu, S.; Huang, S.; Sellinger, I.; Ortiz, M.; Jin, Y.; Lee, S.-H.; Zhang, W., Crystalline Lithium Imidazolate Covalent Organic Frameworks with High Li-Ion Conductivity. *J. Am. Chem. Soc.* **2019,** *141* (18), 7518-7525.
7. Xie, Z.; Wang, B.; Yang, Z.; Yang, X.; Yu, X.; Xing, G.; Zhang, Y.; Chen, L., Stable 2D Heteroporous Covalent Organic Frameworks for Efficient Ionic Conduction. *Angew. Chem. Int. Ed.* **2019,** *58* (44), 15742-15746.
8. Guo, Z.; Zhang, Y.; Dong, Y.; Li, J.; Li, S.; Shao, P.; Feng, X.; Wang, B., Fast Ion Transport Pathway Provided by Polyethylene Glycol Confined in Covalent Organic Frameworks. *J. Am. Chem. Soc.* **2019,** *141* (5), 1923-1927.
9. Jeong, K.; Park, S.; Jung, G. Y.; Kim, S. H.; Lee, Y.-H.; Kwak, S. K.; Lee, S.-Y., Solvent-Free, Single Lithium-Ion Conducting Covalent Organic Frameworks. *J. Am. Chem. Soc.* **2019,** *141* (14), 5880-5885.
10. Zhang, G.; Hong, Y.-L.; Nishiyama, Y.; Bai, S.; Kitagawa, S.; Horike, S., Accumulation of Glassy Poly(ethylene oxide) Anchored in a Covalent Organic Framework as a Solid-State Li^+ Electrolyte. *J. Am. Chem. Soc.* **2019,** *141* (3), 1227-1234.